Volume 52
Number 16
28 April 2023
Pages 4987-5384

Dalton Transactions

An international journal of inorganic chemistry

rsc.li/dalton

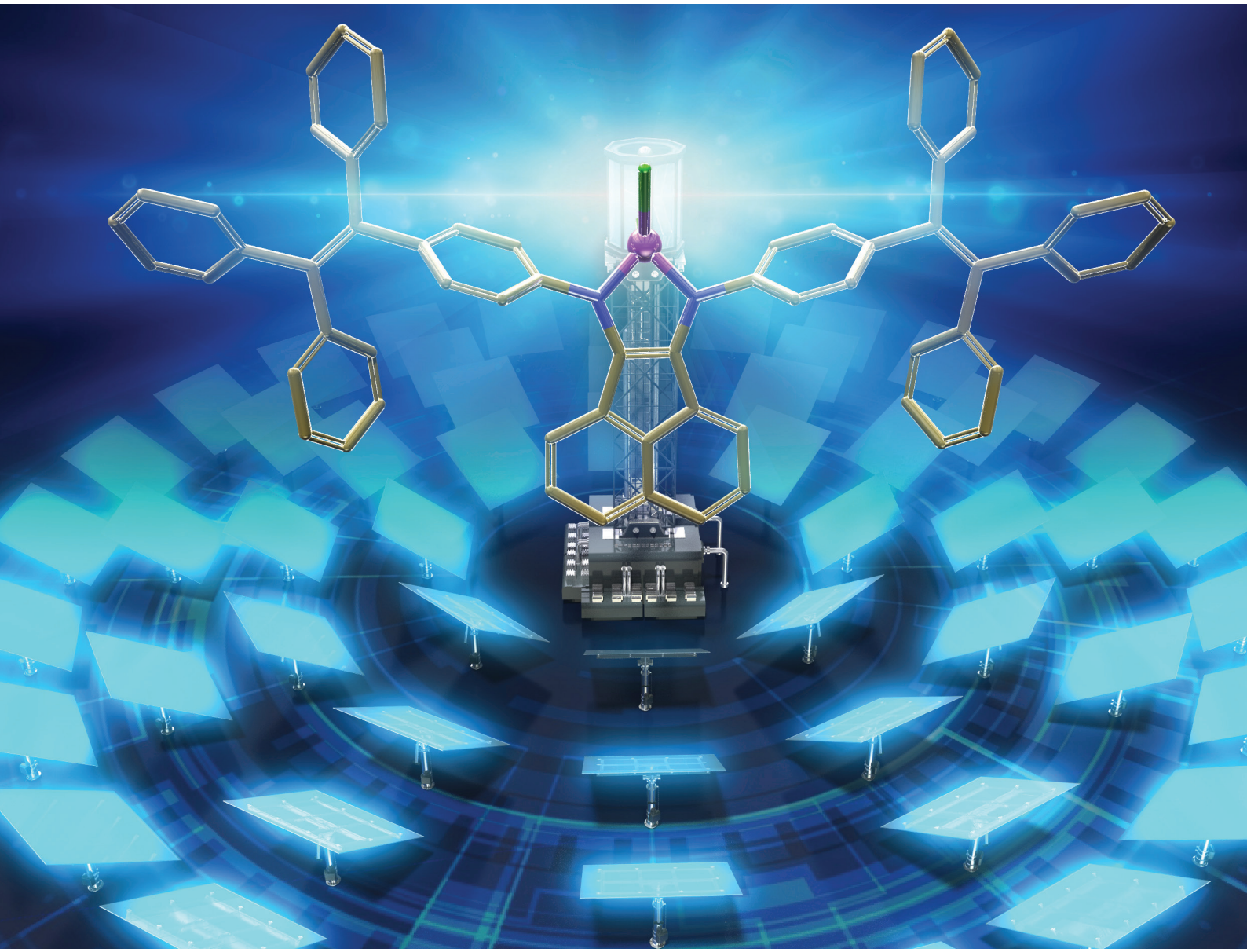

ISSN 1477-9226

ROYAL SOCIETY OF CHEMISTRY

PAPER

Ryo Tanaka, Yousuke Ooyama *et al.*

Aggregation-induced emission of a bis(imino)acenaphthene zinc complex with tetraphenylethene units

Dalton Transactions

ROYAL SOCIETY OF CHEMISTRY

PAPER

View Article Online
View Journal | View Issue

Check for updates

Cite this: *Dalton Trans.*, 2023, **52**, 5047

Aggregation-induced emission of a bis(imino) acenaphthene zinc complex with tetraphenylethene units†

Takuma Fumoto, Ryo Tanaka * and Yousuke Ooyama *

Using bis(imino)acenaphthene (BIAN) zinc(II) and palladium(II) complexes with tetraphenylethene (TPE) units as bulky aryl groups, **Zn-2** and **Pd-2** have been designed and developed, and their photophysical properties in solution and in the solid state have been investigated. Both in solution and in the solid state **Zn-2** and **Pd-2** show two photoabsorption bands in the ranges of 300 nm to 350 nm and 450 nm to 600 nm, which are assigned to the π–π* transition originating from both the TPE units and naphthalene units and the intraligand charge transfer (ILCT) between the TPE units and the BIAN unit, respectively. Density functional theory (DFT) calculations demonstrated that for **Zn-2** the highest occupied molecular orbitals (HOMO) are localized on the TPE units, while the lowest unoccupied molecular orbitals (LUMO) are localized on the BIAN unit, leading to the appearance of a photoabsorption band on the ILCT. The emission from **Zn-2** was quenched in solution, but appeared as phosphorescence at around 600 nm by photoexcitation at the ILCT band in the solid state as well as in the aggregated state, which was formed by the addition of *n*-hexane as a poor solvent to the dichloromethane (DCM) solution. The aggregate formation of **Zn-2** in the DCM/*n*-hexane (10 wt%/90 wt%) solution was confirmed by the Tyndall scattering and scanning electron microscopy (SEM) measurements, demonstrating the aggregation-induced emission (AIE) characteristics of **Zn-2**. On the other hand, **Pd-2** was non-emissive in the solid state and in the aggregated state as well as in solution. Moreover, the DCM-inclusion complexes of **Zn-2** and **Pd-2** were obtained and their photophysical properties were investigated. It was found that the photoluminescence quantum yield ($\Phi_{PL\text{-}solid}$) values of **Zn-2** and **Zn-2-DCM** in the solid state are less than 1%. Single-crystal X-ray structural analysis of **Zn-2-DCM** revealed the absence of intermolecular π–π interactions. Consequently, it was suggested that the low $\Phi_{PL\text{-}solid}$ value of **Zn-2** is mainly due to the radiationless relaxation of the excitons by dynamic rotation of the phenyl groups of the TPE units, even in the solid state and in the aggregation state.

Received 1st November 2022,
Accepted 8th February 2023

DOI: 10.1039/d2dt03525a

rsc.li/dalton

Open Access Article. Published on 08 ubat 2023. Downloaded on 12.07.2024 02:43:51.
This article is licensed under a Creative Commons Attribution 3.0 Unported Licence.

Introduction

Aggregation-induced emission (AIE) is a photophysical phenomenon of luminescent dyes in the aggregation state: the emission enhancement is induced by the formation of dye aggregates usually upon the addition of a poor solvent to the solution.[1–27] Tetraphenylethene (TPE), diphenyldibenzofulvene (DPDBF), and their derivatives are typical AIE-active fluorophores and their AIE mechanisms have been intensely investigated not only to gain new insight into photochemistry but also to explore their practical application.[7–20] It was found that TPE- and DPDBF-based compounds in dilute solutions exhibited almost no emission due to the radiationless (non-emissive) relaxation of the excitons by dynamic rotation of the phenyl groups, but upon aggregate formation by the addition of a poor solvent to the solutions, they exhibit AIE characteristics due to the elimination of the radiationless relaxation by the restricted intramolecular rotation (RIR) of the phenyl groups. Therefore, AIE-active compounds have the potential to be applied to emitters of organic light-emitting diodes (OLEDs), chemo- and biosensors, and two-photon absorption materials,[21–27] unlike the majority of organic emissive dyes, which exhibit aggregation-caused quenching (ACQ) due to the delocalization of excitons or excimers upon the formation of intermolecular π–π interactions between the dye molecules in the solid state. On the other hand, there are reports on AIE of metal complexes[28–37] such as cyclometalated iridium(III) or platinum(II) complexes,[29–33] tricarbonyl rhenium(I) complex,[34] and bis(imino)acenaphthene (BIAN) zinc(II) complexes,[35–37]

Applied Chemistry Program, Graduate School of Advanced Science and Engineering, Hiroshima University, 1-4-1 Kagamiyama, Higashi-Hiroshima 739-8527, Japan. E-mail: rytanaka@hiroshima-u.ac.jp, yooyama@hiroshima-u.ac.jp

†Electronic supplementary information (ESI) available. CCDC 2215754 and 2215755. For ESI and crystallographic data in CIF or other electronic format see DOI: https://doi.org/10.1039/d2dt03525a

Open Access Article. Published on 08 ubat 2023. Downloaded on 12.07.2024 02:43:51.
This article is licensed under a Creative Commons Attribution 3.0 Unported Licence.

although the number of AIE-active metal complexes is smaller than that of AIE-active organic dyes. These studies suggested that the AIE mechanism of metal complexes may be attributed to the restrictions of intramolecular rotation of the ligand and the formation of intermolecular π–π interactions between ligands in the neighboring metal complexes, which inhibit the radiationless relaxation from the metal-to-ligand charge transfer (MLCT), ligand-to-metal charge transfer (LMCT), ligand-to-ligand charge transfer (LLCT) or intraligand charge transfer (ILCT) excited state, resulting in the expression of phosphorescence or fluorescence emission in the aggregated state. In particular, Cowley *et al.* have reported the synthesis and solid-state photoluminescence properties of a series of aryl-substituted BIAN Zn(II) complexes.[36,37] They demonstrated that the emissions from these BIAN Zn complexes were quenched in solution but they became emissive only in the aggregated state. Moreover, it was discovered that these BIAN Zn complexes exhibit solvatomorphism, that is, a change in the solid-state photoluminescence upon inclusion of solvent molecules in the crystal lattice. These interesting results inspired us to conceive BIAN metal complexes with sterically bulky aryl groups in order to gain further insight into substituent effects on the photoluminescence properties both in solution and in the solid state as well as the AIE characteristics.

Thus, in this work, we designed and developed **Zn-2** and **Pd-2** as BIAN zinc(II) and palladium(II) complexes with TPE units as more bulky aryl groups (Scheme 1) and their photophysical properties in solution and in the solid state have been investigated. It was found that the emission from **Zn-2** was quenched in solution, but appeared as phosphorescence upon photoexcitation at the ILCT band in the crystalline state as well as in the aggregated state. On the other hand, **Pd-2** was non-emissive in the crystalline state and in the aggregated state as well as in solution. Moreover, the dichloromethane (DCM)-inclusion complexes of **Zn-2** and **Pd-2** were obtained and their photophysical properties were investigated. Density functional theory (DFT) calculations and single-crystal X-ray structural analysis were performed to elucidate the effects of the molecular packing structure on the solid-state photophysical properties as well as the ILCT of **Zn-2** and **Pd-2**. Herein we report the AIE characteristics of BIAN metal complexes with TPE substituents as bulky aryl groups.

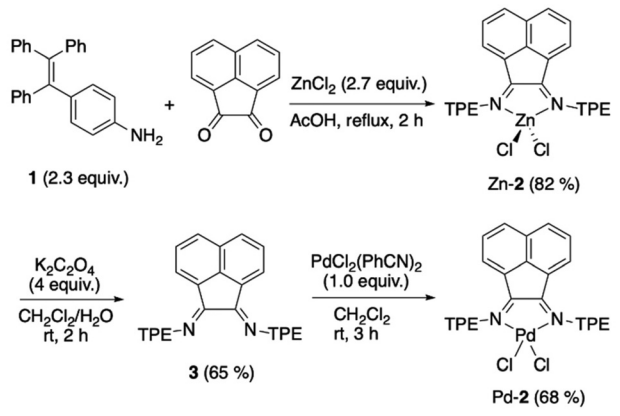

Scheme 1 Synthesis of bis(imino)acenaphthene complexes bearing tetraphenylethene units **Zn-2** and **Pd-2**.

Results and discussion

Synthesis of the BIAN metal complexes Zn-2 and Pd-2 bearing TPE units

Zinc complexes bearing a BIAN ligand are synthesized *via* single-step condensation in the presence of zinc chloride. This method is applicable for versatile starting materials, including sterically demanding anilines.[38] Tetraphenylethylene-substituted aniline **1** cleanly reacted with a 0.5 equivalent of acenaphthenequinone and excess zinc chloride upon refluxing in acetic acid and gave the desired complex **Zn-2**. An analytically pure **Zn-2** was obtained in a high yield by simple filtration and washing the precipitate with acetic acid and ether (Scheme 1). The obtained complex **Zn-2** is stable as a CH_2Cl_2 solution under air for at least one week.

Free BIAN ligand **3** was obtained by the demetallation of **Zn-2** using potassium oxalate as a chelating scavenger of zinc. The obtained **3** can be used for further complexation without any purification. **3** was well soluble in CH_2Cl_2 and chloroform, whereas ether, hexane, and methanol did not solubilize **3**.

Direct synthesis of the free BIAN ligand **3** was also attempted, but the second imine condensation did not proceed, similarly to the other previous examples.[39,40] In the ^{1}H NMR spectrum of the crude product after refluxing acenaphthenequinone and excess aniline **1**, a series of five signals at 8.18, 8.16, 8.04, 7.82, and 7.50 ppm, which are assigned to the asymmetric structure of the acenaphthene skeleton, were observed. These signals typically indicate the formation of monosubstituted imine (see Fig. S6, ESI†).

For comparison with the zinc complex **Zn-2**, a palladium analogue **Pd-2** was synthesized. A reaction of bis(benzonitrile) palladium dichloride with free ligand **3** at room temperature gave **Pd-2** in a high yield (68%). This complex showed sparing solubility in many polar solvents such as CH_2Cl_2, chloroform, THF, and DMSO.

Single-crystal X-ray structural analysis of Zn-2-DCM and Pd-2-DCM

A single crystal of **Zn-2** suitable for X-ray structural analysis was grown by layering hexane on the CH_2Cl_2 solution. The obtained brown plate crystal contained at least one CH_2Cl_2 solvate in the crystal packing (Fig. 1). However, we cannot locate other solvates in the crystal cell because of the severe disorder. The ^{1}H NMR spectrum showed that the crystal contains 1.7 equivalent of CH_2Cl_2 as a solvate. The chemical shifts corresponding to **Zn-2** do not change from the non-solvated **Zn-2** (see Fig. S3†). Thus, this crystal with solvate would show almost the same properties as unsolvated **Zn-2** in solution. Generally, in metal complexes bearing BIAN ligands, the torsion angle between the acenaphthene skeleton and aryl

 This journal is © The Royal Society of Chemistry 2023

Open Access Article. Published on 08 ubat 2023. Downloaded on 12.07.2024 02:43:51.
This article is licensed under a Creative Commons Attribution 3.0 Unported Licence.

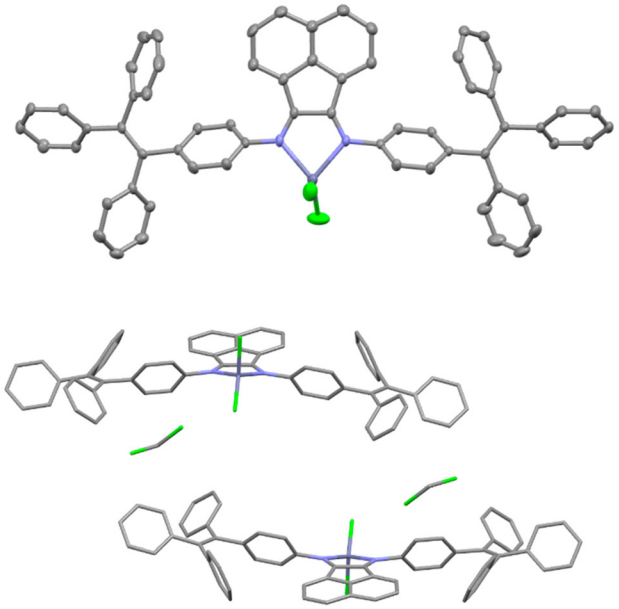

Fig. 1 ORTEP diagram with 50% thermal ellipsoid (top) and crystal packing diagram (bottom) of **Zn-2-DCM**.

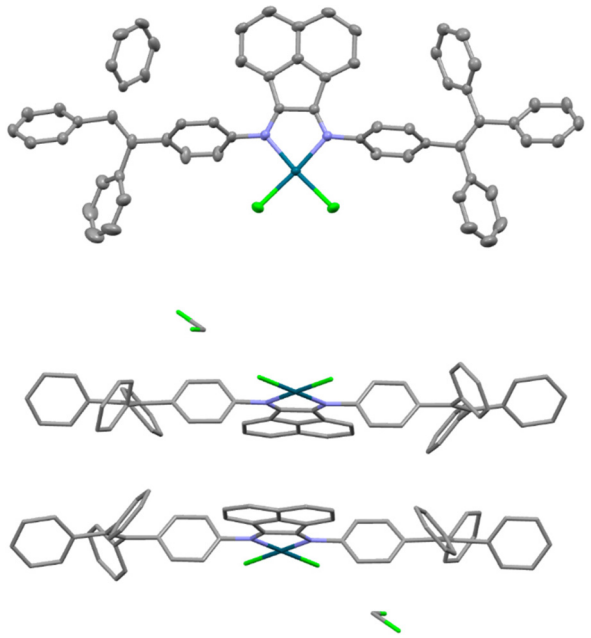

Fig. 2 ORTEP diagram with 50% thermal ellipsoid (top) and crystal packing diagram (bottom) of **Pd-2-DCM**.

groups on the nitrogen atom strongly depends on the bulkiness of aryl groups. In **Zn-2-DCM** the torsion angle of the C–C–N–C bond was 55.0(4)°, which is a significantly low value compared with other BIAN complexes ever reported. This result indicated that the rotation of the TPE unit in solution is not prohibited by the steric effect. The average distance of two Zn–Cl bonds was 2.186(2) Å, the smallest among the previously reported zinc complexes (2.196–2.218 Å).[37] The Zn–Cl bond is short probably because the TPE-containing diimine ligand possesses a relatively low electron-donating ability. In the crystal packing of **Zn-2-DCM**, there are no short π–π contacts of less than 3.60 Å between the aromatic rings in neighboring molecules which indicates the absence of the π–π interactions between the molecules. Photophysical properties derived by the intermolecular interaction are thus not likely in a solid state as discussed later.

A single crystal of **Pd-2-DCM** was grown from the CH_2Cl_2/hexane solution in the same way as **Zn-2-DCM**. The crystal contains at least one dichloromethane solvate and further analysis was not possible because of the severe disorder of solvates (Fig. 2). The crystal was so brittle in mineral oil that it can collapse in a few minutes at room temperature, probably because solvates are easily eliminated to mineral oil. Unlike tetrahedral **Zn-2-DCM**, **Pd-2-DCM** showed a square planar structure as most of the 4-coordinated palladium complexes. The torsion angle between the acenaphthene ring and aryl groups was 66.0(3)°, slightly larger than that of **Zn-2-DCM** because of the steric effect of chlorides. Any π–π interaction between the TPE units and the BIAN unit in neighboring molecules was observed in the crystal packing of **Pd-2-DCM**.

Meanwhile, unfortunately, we could not obtain guest solvent-free single crystals of **Zn-2** and **Pd-2** to make the X-ray structural analysis possible.

Photophysical properties of Zn-2 and Pd-2 in solution

The photoabsorption and photoluminescence spectra of the free BIAN ligand **3** as well as **Zn-2** and **Pd-2** in DCM are shown in Fig. 3, and their photophysical data are summarized in Table 1. The free BIAN ligand **3**, **Zn-2**, and **Pd-2** show two photoabsorption bands. A relatively narrow band ($\lambda_{max}^{abs-solution}$ = *ca.* 310 nm) with a high molar extinction coefficient (ε_{max}) value (*ca.* 30 000–35 000 M^{-1} cm^{-1}) in the range of 300 nm to

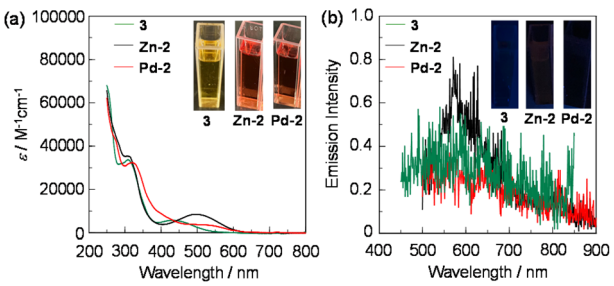

Fig. 3 (a) Photoabsorption (10^{-4}–10^{-5} M) and (b) emission spectra (1.0 × 10^{-4} M, λ^{ex} = 430 nm for **3** and 490 nm for **Zn-2** and **Pd-2**) of **3**, **Zn-2** and **Pd-2** in dichloromethane.

Table 1 Photophysical data of **3**, **Zn-2** and **Pd-2** in dichloromethane

Complex	$\lambda_{max}^{abs-solution}$/nm ($\varepsilon_{max}$/$M^{-1}$ cm^{-1})	$\lambda_{max}^{PL-solution}$/nm
3	308 (33 800), 433 (5800)	—[a]
Zn-2	306 (35 500), 490 (8400)	580
Pd-2	321 (32 400), 480[br] (4000)	—[a]

[a] Too weak.

Open Access Article. Published on 08 ubat 2023. Downloaded on 12.07.2024 02:43:51.
This article is licensed under a Creative Commons Attribution 3.0 Unported Licence.

350 nm is assigned to the π–π* transition originating from both the TPE units and naphthalene units. The other broad band ($\lambda_{max}^{abs-solution}$ = 433 nm for **3** and *ca.* 485 nm for **Zn-2**, and **Pd-2**) with a relatively low ε_{max} value (*ca.* 4000–8000 M^{-1} cm^{-1}) in the range of 400 nm to 600 nm is ascribable to the intraligand charge transfer (ILCT) between the TPE units and the BIAN unit, and the ILCT bands of **Zn-2** and **Pd-2** showed the bathochromic shift by *ca.* 50 nm in comparison with that of **3**, which are also supported by the TD-DFT calculations as discussed later. Interestingly, the ILCT bands of **3** and **Zn-2** are of a clear shape with a relatively high ε_{max} value, compared to that of **Pd-2**. On the other hand, for the corresponding photoluminescence spectra by photoexcitation (λ^{ex} = 490 nm) at the ILCT band, **Zn-2** exhibited an extremely feeble emission band at around 580 nm (photoluminescence quantum yield ($\Phi_{PL\text{-}solution}$) was not determinable) which is assignable to phosphorescence as discussed later on, while **3** and **Pd-2** were non-emissive in the DCM solution. Moreover, it was found that the photoluminescent spectrum of **Zn-2** in the glassy matrix (frozen solution) of 2-MeTHF at 77 K exhibits intense emission, compared to that in 2-MeTHF at 298 K, but **3** and **Pd-2** were non-emissive even in the glassy matrix of 2-MeTHF at 77 K (Fig. S12, ESI†). The difference in photoabsorption and photoluminescence properties between **Zn-2** and **Pd-2** may be due to the different coordination geometry and heavy atom effect. As shown in the insets of Fig. 3a and b, one can see that in the DCM solution **Zn-2** and **Pd-2** are orange, and **Zn-2** exhibited an extremely feeble red emission while **Pd-2** is non-emissive.

DFT study of Zn-2 and Pd-2 and the free ligand 3

DFT calculations were performed on the complex **Zn-2** and **Pd-2** and free ligand **3** to assign the electron transitions in the visible region. Geometry optimizations for **Zn-2** and **Pd-2** were performed starting from the crystal structure, and the located structures at their local minima of energy were almost the same as the crystal structure. Single point energy calculations for the optimized geometry of **Zn-2** and **Pd-2**, calculated with the larger basis sets (cc-pVTZ-pp for palladium and cc-pVTZ for the other atoms) demonstrated that the highest occupied molecular orbitals (HOMO) are localized on the TPE units, while the lowest unoccupied molecular orbitals (LUMO) are localized on the BIAN unit (Fig. 4, Fig. S9 and S10, ESI†).

In time-dependent density functional theory (TD-DFT) calculations, the empirical dispersion correction was applied. The consideration of dispersion correction has previously reproduced the UV-vis spectra of a series of BIAN Ni complexes.[41,42] For **Zn-2**, the $S_0 \rightarrow S_1$ transition is solely attributed to the transition (oscillator strength (f) = 0.35) from the HOMO to the LUMO (Table S2, ESI†), leading to the appearance of a photoabsorption band on the ILCT from the TPE units to the BIAN unit. **Pd-2** showed a similar absorption band for the $S_0 \rightarrow S_1$ transition with a lower oscillator strength (Table S3, ESI,† (f) = 0.13). Besides the HOMO–LUMO transition, the transition from HOMO−2 to LUMO was slightly contributed (13%). The smaller oscillator strength in **Pd-2** than in **Zn-2** nicely reproduces the weaker photoabsorption spectrum in solution.

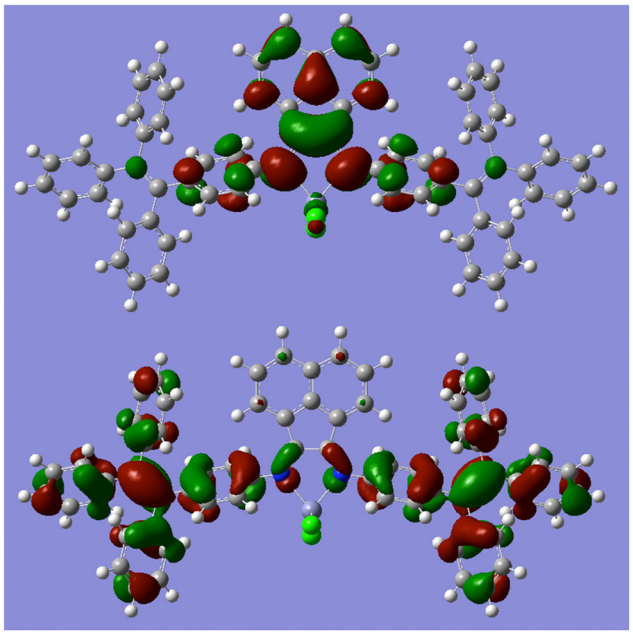

Fig. 4 HOMO (bottom) and LUMO (top) of **Zn-2** derived from DFT calculations at the cc-pVTZ level.

However, the calculated energy gap for both $S_0 \rightarrow S_1$ transitions (1.59 eV for **Zn-2** and 1.50 eV for **Pd-2**) showed about 1 eV smaller than that estimated from the experimental photoabsorption spectrum (2.53 eV for **Zn-2** and 2.58 eV for **Pd-2**) in DCM. Such differences between the theoretical and experimental results are also observed in the other zinc complexes,[36,37] which is probably attributed to the excitation regarding multiple orbitals.

The starting point of geometry optimization for ligand **3** was located according to the crystal structure of **Zn-2**, and the conformation of the local minimum was similar to that ligated to zinc or palladium. The TD-DFT study of **3** showed a much lower excitation energy for the $S_0 \rightarrow S_1$ transition (2.10 eV), which is attributed to the HOMO–LUMO transition (Table S4, ESI†). The tendency of the calculated excitation energies of **Zn-2** and ligand **3** was in agreement with the photoabsorption band in solution.

We also evaluated the $S_0 \rightarrow T_1$ transition of **Zn-2** and **Pd-2** using TD-DFT because the emissions previously reported for zinc-diimine complexes are proposed as phosphorescence. For both complexes, transitions with a lower excitation energy than the singlet state (1.32 eV for **Zn-2** and 1.28 eV for **Pd-2**) were found (Table S5, ESI†). The optimized geometries of triplet species using the U-DFT method showed almost the same energy as the excited state calculated by TD-DFT (Table S7, ESI†). However, the origin of the emission from **Zn-2** cannot be revealed only by DFT studies because of the large difference in the calculated excitation energy and experimental emission band.

This journal is © The Royal Society of Chemistry 2023

Open Access Article. Published on 08 ubat 2023. Downloaded on 12.07.2024 02:43:51.
This article is licensed under a Creative Commons Attribution 3.0 Unported Licence.

Photophysical properties of Zn-2, Pd-2 and Zn-2-DCM in the solid state

The solid-state UV-Vis diffuse reflection–photoabsorption, photoexcitation and photoluminescence spectra of the free BIAN ligand **3** as well as **Zn-2**, **Pd-2** and **Zn-2-DCM** are shown in Fig. 5; unfortunately, we could not perform the spectral measurements of **Pd-2-DCM** due to the easy release of DCM from the inclusion crystal under the atmosphere at room temperature. As with the case of the DCM solutions, **Zn-2** and **Pd-2** in the solid state show two photoabsorption bands in the ranges of 300 nm to 400 nm and 400 nm to 600 nm, originating from both the TPE units and naphthalene units and the ILCT, respectively, while the photoabsorption bands in the solid state were broadened in comparison with those in DCM (Fig. 5a). The photoabsorption band of **Zn-2-DCM** (λ_{max}^{abs} = 519 nm) showed the bathochromic shift by *ca.* 40–50 nm in comparison with those of **3** and **Zn-2**. For the corresponding photoluminescence spectra, **Zn-2** exhibited a clear photoluminescence band with the maximum ($\lambda_{max}^{PL-solid}$) at 580 nm by λ^{ex} at 510 nm in comparison with the case of **Zn-2** in DCM, while the photoluminescence band ($\lambda_{max}^{PL-solid}$ = 660 nm by λ^{ex} at 520 nm) of **Zn-2-DCM** appeared in a longer wavelength region by *ca.* 80 nm in comparison with that of **Zn-2** (Table 2). However, the $\Phi_{PL\text{-}solid}$ values of **Zn-2** and **Zn-2-DCM** in the solid state were found to be less than 1.0%. Meanwhile, **3** and **Pd-2** in the solid state were non-emissive as with the case of the DCM solution (Fig. 5b). The photoexcitation spectra of **Zn-2** and **Zn-2-DCM** appeared at a wavelength range similar to their photoabsorption spectra, although the photoexcitation maxima of **Zn-2** and **Zn-2-DCM** showed the bathochromic shift and the hypsochromic shift (Fig. S13, ESI†), respectively, by *ca.* 40–50 nm in comparison with their photoabsorption spectra. Considering the absence of the intermolecular π–π interactions affecting the solid-state photophysical properties which have been revealed by the single-crystal X-ray structural analysis of **Zn-2-DCM**, the significantly low $\Phi_{PL\text{-}solid}$ values of **Zn-2** and **Zn-2-DCM** compared to those of aryl-substituted BIAN Zn complexes[36,37] reported by Cowley *et al.* may be attributed to the radiationless relaxation of the excitons by dynamic rotation of the phenyl groups of the TPE units, even in the solid state and in the aggregated state. In order to further reveal the luminescence characteristics of the BIAN Zn complex with TPE units, we have performed time-resolved photoluminescence spectroscopy for **Zn-2** and **Zn-2-DCM**. However, for both **Zn-2** and **Zn-2-DCM** the precise evaluation of the emission lifetime ($\tau_{PL\text{-}solid}$) value was difficult due to their feeble solid-state luminescence properties. Nevertheless, based on the fact reported by Cowley *et al.* that emissions from aryl-substituted BIAN Zn complexes were identified as being phosphorescent with microsecond lifetimes at room temperature,[37] the emissions from **Zn-2** and **Zn-2-DCM** in the solid state are also assignable to phosphorescence. As shown in the insets of Fig. 6, in the solid state, the colours are yellowish orange for **Zn-2** and orange for **Pd-2** and **Zn-2-DCM**, and the luminescent colours are orange for **Zn-2** and red for **Zn-2-DCM**.

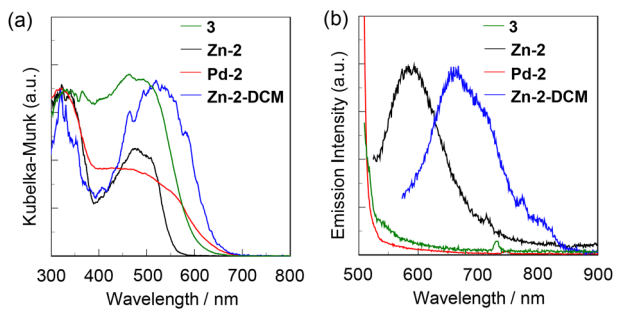

Fig. 5 (a) Solid-state UV-vis diffuse reflection–absorption and (b) emission spectra (λ^{ex} = 490–520 nm) of **3**, **Zn-2**, **Pd-2**, and **Zn-2-DCM** in the solid state.

Table 2 Photophysical data of **Zn-2**, **Zn-2-DCM**, and **Pd-2** in the solid state

Complex	$\lambda_{max}^{abs-solid}$/nm	$\lambda_{max}^{PL-solid}$/nm
3	325, 464	—[a]
Zn-2	322, 475	584
Pd-2	318, 480[br]	—[a]
Zn-2-DCM	320, 519	660

[a] Not detectable.

Aggregation-induced emission of Zn-2

The AIE characteristics of **Zn-2** were investigated by photoabsorption and photoluminescence spectral measurements of the DCM/*n*-hexane mixture by the addition of *n*-hexane as a poor solvent to the DCM solution of **Zn-2** (Fig. 7a and b). In the hexane fraction range below *ca.* 70 wt% (in the DCM/*n*-hexane mixture over *ca.* 30 wt% DCM fraction), the photoabsorption and photoluminescence spectra (λ^{ex} = 490 nm) of **Zn2** showed unnoticeable changes. In the range of 80–90 wt% hexane fraction (in a 20–10 wt% DCM fraction), the photoabsorption band showed a decrease in the absorbance, indicating the formation of aggregates. For the corresponding photoluminescence spectra, on the other hand, the photoluminescence band with the maximum ($\lambda_{max}^{PL-solid}$) at 620 nm appeared at 90 wt% hexane fraction (at 10 wt% DCM fraction), which is assignable to phosphorescence as with the case of **Zn-2** in the solid state. Interestingly, the photoluminescence band of **Zn-2** in its aggregated state appeared at a longer wavelength region by 36 nm than that in the solid state. The differences in the photophysical properties between the solid state

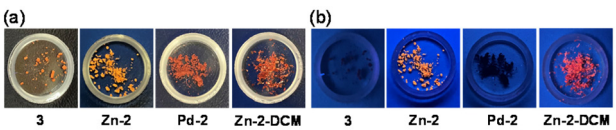

Fig. 6 Photographs of solids of **3**, **Zn-2**, **Pd-2**, and **Zn-2-DCM** under (a) room light and (b) UV-light (365 nm) irradiation.

Open Access Article. Published on 08 ubat 2023. Downloaded on 12.07.2024 02:43:51.
This article is licensed under a Creative Commons Attribution 3.0 Unported Licence.

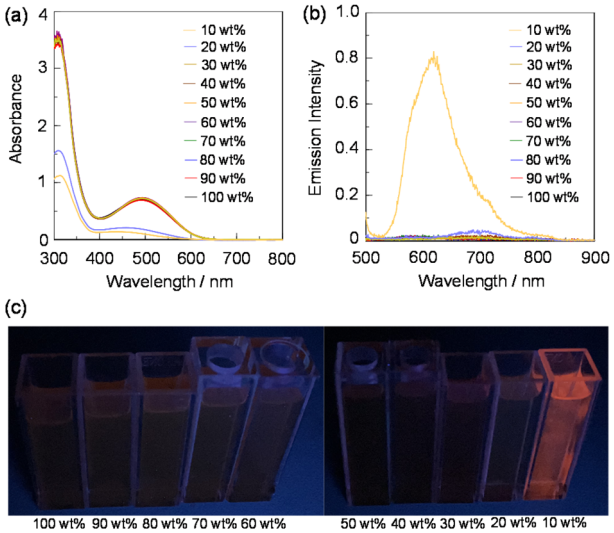

Fig. 7 (a) Photoabsorption and (b) emission spectra (λ^{ex} = 490 nm), and (c) photographs (under UV-light (365 nm) irradiation) of **Zn-2** (1.0×10^{-4} M) in a dichloromethane/*n*-hexane mixture (10–100 wt% for the dichloromethane fraction).

and the aggregated state may be attributed to the differences in the molecular arrangement and/or the intermolecular interaction between them. As shown in Fig. 7c, red luminescence can be observed by the naked eye for the DCM/*n*-hexane (10 wt%/90 wt%) solution under 365 nm irradiation. The aggregate formation of **Zn-2** in the 80–90 wt% hexane fraction (in the 20–10 wt% DCM fraction) was confirmed by the Tyndall scattering (Fig. 8a) and scanning electron microscopy (SEM) measurements (Fig. 8b). Indeed, the SEM image displayed the formation of the micrometer-sized aggregates. On the other hand, **Pd-2** was non-emissive in the aggregated state as with the case in the solid state.

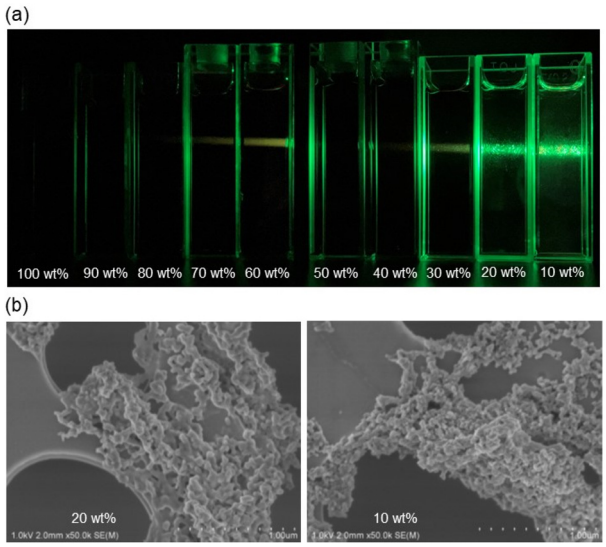

Fig. 8 (a) Tyndall scattering of **Zn-2** (1.0×10^{-4} M) in a dichloromethane/*n*-hexane mixture (10–100 wt% for the dichloromethane fraction) under irradiation with a laser beam. (b) SEM images of substances obtained from the dichloromethane/*n*-hexane solution of **Zn-2** with 20 wt% and 10 wt% dichloromethane fractions.

Conclusions

In order to investigate the photophysical properties of bis(imino)acenaphthene (BIAN) metal complexes with sterically bulky aryl groups both in solution and in the solid, we designed and developed BIAN Zn(II) and Pd(II) complexes (**Zn-2** and **Pd-2**) with tetraphenylethene (TPE). Both in solution and in the solid state **Zn-2** and **Pd-2** showed two photoabsorption bands in the ranges of 300 nm to 350 nm and 450 nm to 600 nm, which are assigned to the π–π* transition originating from both the TPE units and naphthalene units and the intraligand charge transfer (ILCT) between the TPE units and the BIAN unit, respectively. It was found that the emission from **Zn-2** was quenched in solution, but it appeared as phosphorescence upon photoexcitation at the ILCT band in the solid state. Moreover, the aggregation-induced emission (AIE) characteristics of **Zn-2** were observed in the dichloromethane/*n*-hexane (10 wt%/90 wt%) solution. However, the photoluminescence quantum yield ($\Phi_{PL\text{-}solid}$) of **Zn-2** in the solid state was found to be less than 1.0%. On the other hand, **Pd-2** was non-emissive in the solid state and in the aggregated state as well as in solution. The single-crystal X-ray structural analysis of the dichloromethane-inclusion complexes of **Zn-2** and **Pd-2** revealed the absence of the intermolecular π–π interactions affecting their solid-state photophysical properties. It was found that the low $\Phi_{PL\text{-}solid}$ value of **Zn-2** is mainly due to the radiationless relaxation of the excitons by dynamic rotation of the phenyl groups of the TPE units, even in the solid state and in the aggregated state. Consequently, this work provides new insight into substituent effects on the photoluminescence properties of BIAN Zn(II) complexes.

Experimental

General

All the oxygen and moisture-sensitive materials were prepared and handled under a dry nitrogen atmosphere using standard Schlenk techniques. Aniline **1** was prepared according to the literature.[43] Dry toluene, dichloromethane, and ether for synthesis (Kanto Chemical Co.) were purified by passing through a degassed column and stored over molecular sieves 3A. Other materials were used as received. Recycling gel permeation chromatography (GPC) was performed using an RI-detector (GL Science RI 704), a pump (GILSON 307 PUMP), and two columns (Shodex GPC H-2001L). NMR spectra were recorded on a Varian System 500 spectrometer. The obtained spectra are referenced to the residual signals of the partially protonated solvent [^{1}H: δ = 7.26 ppm ($CHCl_3$)] or solvent [^{13}C: δ = 77.16 ppm ($CDCl_3$)]. High-resolution mass spectrometry of new compounds was performed on a JEOL JMS-T100GCV

This journal is © The Royal Society of Chemistry 2023

Open Access Article. Published on 08 ubat 2023. Downloaded on 12.07.2024 02:43:51.
This article is licensed under a Creative Commons Attribution 3.0 Unported Licence.

(GC-FD) or a Thermo Fisher LTQ Orbitrap XL spectrometer (ESI). The photoabsorption spectra of solutions were recorded with a Shimadzu UV-3600 plus spectrophotometer. The photoabsorption spectra of solids were recorded using a Shimadzu UV-3600 plus spectrophotometer with a calibrated integrating sphere system. Photoluminescence spectra were measured with a Hitachi F-4500 spectrophotometer. The luminescence quantum yields were determined using a Hamamatsu C9920-01 equipped with a CCD using a calibrated integrating sphere system. Time-resolved photoluminescence spectroscopy was performed on a HORIBA DeltaFlex modular fluorescence lifetime system, using a Nano LED pulsed diode excitation source. The solid morphology was observed using a Hitachi S-4800 scanning electron microscope (SEM) coupled with an energy-dispersive X-ray (EDX) analyzer. The dispersed samples in solution were dried on a carbon-coated copper grid without any metal coating.

Synthesis of the BIAN-zinc complex (Zn-2)

In a 25 mL test tube, a mixture of acenaphthenequinone (122 mg, 0.67 mmol) and zinc chloride (245 mg, 1.8 mmol) was suspended in acetic acid (6 mL) and heated to 60 °C. Powdered aniline **1** (535 mg, 1.54 mmol) was added to the yellow suspension in 30 portions over 10 minutes, and the mixture was refluxed for 3 hours. The resulting reddish-brown solution was cooled to room temperature, and the generated dark red precipitate was filtered off. The precipitate was sequentially washed with acetic acid (2 mL × 2) and ether (3 mL × 3). The remaining solid was dissolved in dichloromethane (20 mL) and the solvent was removed under reduced pressure. 461 mg (82%) of **Zn-2** was obtained as a brown solid; FD-HRMS: calcd for $C_{64}H_{44}N_2ZnCl_2$ 974.2173; found 974.2161. ^{1}H NMR ($CDCl_3$): δ 8.18 (2H, d, $^3J_{HH}$ = 8 Hz), 7.62 (2H, t, $^3J_{HH}$ = 8 Hz), 7.41 (2H, d, $^3J_{HH}$ = 8 Hz), 7.36 (4H, d, $^3J_{HH}$ = 8 Hz), 7.24–7.06 (34H, brm). ^{13}C NMR ($CDCl_3$): δ 162.2, 145.3, 145.1, 144.1, 143.2, 142.6, 142.4, 141.8, 140.3, 133.1, 132.5, 131.8, 131.5, 131.4, 131.2, 128.7, 128.1, 128.0, 127.9, 127.1, 127.0, 126.8, 126.2, 125.3, 121.5.

Synthesis of the free BIAN ligand 3

In a 100 mL round-bottomed flask, the zinc complex **Zn-2** (362 mg, 0.37 mmol) was dissolved in dichloromethane (10 mL). To the brown solution, an aqueous solution of potassium oxalate (276 mg, 1.5 mmol in 5 mL) was added dropwise and the mixture was vigorously stirred for 2 hours at room temperature. The separated organic phase was washed three times with 10 mL of water, dried under magnesium sulfate and dried under reduced pressure. 203 mg (65%) of **3** was obtained as an orange powder; ESI-MS: calcd for $C_{64}H_{44}N_2$ 841.3583 [M + H]; found 841.3581. ^{1}H NMR ($CDCl_3$): δ 7.94 (2H, d, $^3J_{HH}$ = 8 Hz), 7.45 (2H, t, $^3J_{HH}$ = 8 Hz), 7.22–7.05 (34H, brm), 6.98 (2H, d, $^3J_{HH}$ = 8 Hz), 6.88 (4H, d, $^3J_{HH}$ = 8 Hz). ^{13}C NMR ($CDCl_3$): δ 161.0, 149.9, 144.3, 143.8, 143.7, 141.9, 141.1, 141.0, 140.3, 132.5, 131.7, 131.5, 131.5, 131.3, 129.1, 128.8, 127.8, 127.7, 126.7, 126.6, 126.5, 124.2, 118.0. Two aromatic peaks would be overlapped with other peaks.

Attempt at the direct synthesis of the BIAN ligand 3

In a 20 mL Schlenk flask, aniline **1** (236 mg, 0.68 mmol), acenaphthenequinone (54 mg, 0.30 mmol), and *p*-toluenesulfonic acid monohydrate (10 mg) were suspended in toluene (6 mL) and heated to 100 °C under nitrogen for 8 hours. The resulting mixture was cooled to room temperature and poured into ether (30 mL). The precipitated solid was collected and dried under vacuum. 213 mg of yellowish solid was obtained. The ^{1}H NMR spectrum indicated that the crude product contains aniline **1** and monosubstituted imine in about a 1 : 1.7 molar ratio.

Synthesis of the BIAN-palladium complex (Pd-2)

In a 20 mL Schlenk flask, ligand **3** (52 mg, 62 μmol) and bis(benzonitrile)palladium dichloride (24 mg, 62 μmol) are weighed and dissolved in 2 mL of dichloromethane. This solution was stirred at room temperature for three hours. The resulting solution was filtered through Celite and the residue was washed three times with 3 mL of dichloromethane under nitrogen. The combined solution was dried under vacuum and the resulting solid was washed three times with 2 mL of ether. 43 mg (68%) of **Pd-2** was obtained as a brown solid; ESI-MS: calcd for $C_{64}H_{44}N_2PdCl_2$ 1016.1916; found 1016.1916. ^{1}H NMR ($CDCl_3$): δ 8.16 (2H, d, $^3J_{HH}$ = 10 Hz), 7.57 (2H, t, $^3J_{HH}$ = 10 Hz), 7.25–7.05 (38H, brm), 6.89 (2H, d, $^3J_{HH}$ = 10 Hz). ^{13}C NMR ($CDCl_3$): δ 174.3, 144.9, 143.6, 143.2, 143.0, 142.9, 142.7, 142.3, 140.0, 132.2, 131.6, 131.4, 131.2, 128.8, 128.0, 127.9, 127.8, 127.5, 126.9, 126.8, 126.7, 126.1, 124.9, 122.2. One aromatic peak would be overlapped with other peaks.

Single-crystal X-ray structural analysis

Single crystals of **Zn-2-DCM** and **Pd-2-DCM** for the X-ray diffraction study, which contain CH_2Cl_2 as a solvate, were obtained from the CH_2Cl_2/hexane solution. X-ray diffraction measurements were performed on a RIGAKU XtaLAB Synergy R/DW diffractometer using Mo Kα radiation (λ = 0.71069 Å; $2\theta_{max}$ = 55.6°; crystal-to-detector distance = 59.5 mm). The structures were resolved using direct methods with SHELXT 2018/2[44] and refined using full-matrix least-squares techniques against F^2 (SHELXL 2018/3).[45] Non-hydrogen atoms were refined anisotropically, while hydrogen atoms were located using AFIX instructions. The contribution of a part of the disordered solvate was corrected using PLATON/SQUEEZE tools.[46] The crystallographic data have been deposited at the Cambridge Crystallographic Data Centre (CCDC 2215754 for **Zn-2-DCM**, CCDC 2215755 for **Pd-2-DCM**†).

Details of the theoretical studies

All the DFT calculations were performed using the (U)TPSSh functional[47] on Gaussian 16 Rev. C01 program.[48] Geometry optimizations were performed starting from the X-ray crystal structures (for **Zn-2** and **Pd-2**) or structures modified from the X-ray structure of **Zn-2** (for **3**), using Lanl2dz(Pd)/cc-pVDZ (other atoms) basis sets. All local minima after geometry optimizations were confirmed by their vibrational frequency

Open Access Article. Published on 08 ubat 2023. Downloaded on 12.07.2024 02:43:51.
This article is licensed under a Creative Commons Attribution 3.0 Unported Licence.

calculations. Single point energy calculations and TD-DFT calculations of the electronic transition energy for the optimized geometries were performed using cc-pVTZ-PP(Pd)/cc-pVTZ (other atoms) basis sets. Grimme's D3 empirical dispersion corrections[49] with Becke–Johnson damping functions[50] were included.

Conflicts of interest

There are no conflicts to declare.

Acknowledgements

This work was supported by the Grants-in-Aid for Scientific Research (B) from the Japan Society for the Promotion of Science (JSPS) KAKENHI Grant Number 22H02123 and the Iketani foundation.

References

1 J. Luo, Z. Xie, J. W. Y. Lam, L. Cheng, H. Chen, C. Qiu, H. S. Kwok, X. Zhan, Y. Liu, D. Zhu and B. Z. Tang, *Chem. Commun.*, 2001, 1740–1741.
2 Y. Hong, J. W. Y. Lama and B. Z. Tang, *Chem. Commun.*, 2009, 4332–4253.
3 J. Mei, N. L. C. Leung, R. T. K. Kwok, J. W. Y. Lam and B. Z. Tang, *Chem. Rev.*, 2015, **115**, 11718–11940.
4 Q. Yan and S. Wang, *Mater. Chem. Front.*, 2020, **4**, 3153–3175.
5 J. Li, J. Wang, H. Li, N. Song, D. Wang and B. Z. Tang, *Chem. Soc. Rev.*, 2020, **49**, 1144–1172.
6 Y. Sun, Z. Lei and H. Ma, *J. Mater. Chem. C*, 2022, **10**, 14834–14867.
7 Y. Zhang, D. Li, Y. Li and J. Yu, *Chem. Sci.*, 2014, **5**, 2710–2716.
8 J. Tong, Y. Wang, J. Mei, J. Wang, A. Qin, J. Z. Sun and B. Z. Tang, *Chem. – Eur. J.*, 2014, **20**, 4661–4670.
9 X. Y. Shen, Y. J. Wang, E. Zhao, W. Z. Yuan, Y. Liu, P. Lu, A. Qin, Y. Ma, J. Z. Sun and B. Z. Tang, *J. Phys. Chem. C*, 2013, **117**(14), 7334–7347.
10 N. Zhao, Z. Yang, J. W. Y. Lam, H. H. Y. Sung, N. Xie, S. Chen, H. Su, M. Gao, I. D. Williams, K. S. Wong and B. Z. Tang, *Chem. Commun.*, 2012, **48**, 8637–8639.
11 F. Khan, A. Ekbote, S. M. Mobin and R. Misra, *J. Org. Chem.*, 2021, **86**, 1560–1574.
12 W. Guan, W. Zhou, C. Lu and B. Z. Tang, *Angew. Chem., Int. Ed.*, 2015, **54**, 15160–15164.
13 J.-B. Xiong, H.-T. Feng, J.-P. Sun, W.-Z. Xie, D. Yang, M. Liu and Y.-S. Zheng, *J. Am. Chem. Soc.*, 2016, **138**, 11469–11472.
14 Q.-Y. Li, Z. Ma, W.-Q. Zhang, J.-L. Xu, W. Wei, H. Lu, X. Zhao and X.-J. Wang, *Chem. Commun.*, 2016, **52**, 11284–11287.
15 X. Liu and G. Liang, *Chem. Commun.*, 2017, **53**, 1037–1040.
16 C. Gui, E. Zhao, R. T. K. Kwok, A. C. S. Leung, J. W. Y. Lam, M. Jiang, H. Deng, Y. Cai, W. Zhang, H. Su and B. Z. Tang, *Chem. Sci.*, 2017, **8**, 1822–1830.
17 Y. Ooyama, M. Sugino, T. Enoki, K. Yamamoto, N. Tsunoji and J. Ohshita, *New J. Chem.*, 2017, **41**, 4747–4749.
18 H. Zhang, Y. Nie, J. Miao, D. Zhang, Y. Li, G. Liu, G. Sun and X. Jiang, *J. Mater. Chem. C*, 2019, **7**, 3306–3314.
19 Y. Mise, K. Imato, T. Ogi, N. Tsunoji and Y. Ooyama, *New J. Chem.*, 2021, **45**, 4164–4173.
20 E. Nishimoto, Y. Mise, T. Fumoto, S. Miho, N. Tsunoji, K. Imato and Y. Ooyama, *New J. Chem.*, 2022, **46**, 12474–12481.
21 R. Furue, T. Nishimoto, I. S. Park, J. Lee and T. Yasuda, *Angew. Chem., Int. Ed.*, 2016, **55**, 7171–7175.
22 H. Lu, Y. Zheng, X. Zhao, L. Wang, S. Ma, X. Han, B. Xu, W. Tian and H. Gao, *Angew. Chem., Int. Ed.*, 2016, **55**, 155–159.
23 H. Naito, K. Nishino, Y. Morisaki, K. Tanaka and Y. Chujo, *Angew. Chem., Int. Ed.*, 2017, **56**, 254–259.
24 C.-J. Zhang, G. Feng, S. Xu, Z. Zhu, X. Lu, J. Wu and B. Liu, *Angew. Chem., Int. Ed.*, 2016, **55**, 6192–6196.
25 H. Tong, Y. Dong, Y. Hong, M. Häussler, J. W. Y. Lin, H. H.-Y. Sung, X. Yu, J. Sun, I. D. Williams, H. S. Kwok and B. Z. Tang, *J. Phys. Chem. C*, 2017, **111**, 2287–2294.
26 C. Gui, E. Zhao, R. T. K. Kwok, A. C. S. Leung, J. W. Y. Lam, M. Jiang, H. Deng, Y. Cai, W. Zhang, H. Su and B. Z. Tang, *Chem. Sci.*, 2017, **8**, 1822–1830.
27 X. Liu and G. Liang, *Chem. Commun.*, 2017, **53**, 1037–1040.
28 P. Prasad, A. Gupta and P. K. Sasmal, *Chem. Commun.*, 2021, **57**, 174–186.
29 C. Jin, J. Liu, Y. Chen, R. Guan, C. Ouyang, Y. Zhu, L. Ji and H. Chao, *Sci. Rep.*, 2016, **6**, 22039.
30 S. K. Sheet, B. Sen, K. Aguan and S. Khatua, *Dalton Trans.*, 2018, **47**, 11477–11490.
31 K. Ohno, T. Sakata, M. Shiiba, A. Nagasawa and T. Fujihara, *Dalton Trans.*, 2019, **48**, 8068–8075.
32 J. Song, M. Wang, X. Xu, L. Qu, X. Zhou and H. Xiang, *Dalton Trans.*, 2019, **48**, 4420–4428.
33 N. F. Romashev, P. A. Abramov, I. V. Bakaev, I. S. Fomenko, D. G. Samsonenko, Al. S. Novikov, K. K. H. Tong, D. Ahn, V. Dorovatovskii, Y. V. Zubavichus, A. A. Ryadun, O. A. Patutina, M. N. Sokolov, M. V. Babak and A. L. Gushchin, *Inorg. Chem.*, 2022, **61**, 2105–2118.
34 J. Wang, A. Poirot, B. Delavaux-Nicot, M. Wolff, S. Mallet-Ladeira, J. P. Calupitan, C. Allain, E. Benoist and S. Fery-Forgues, *Dalton Trans.*, 2019, **48**, 15906–15916.
35 N. J. Hill, I. Vargas-Baca and A. H. Cowley, *Dalton Trans.*, 2009, 240–253.
36 D. A. Evans, L. M. Lee, I. Vargas-Baca and A. H. Cowley, *Organometallics*, 2015, **34**, 2422–2428.
37 D. A. Evans, L. M. Lee, I. Vargas-Baca and A. H. Cowley, *Dalton Trans.*, 2015, **44**, 11984–11996.
38 L. Guo, W. Kong, Y. Xu, Y. Yang, R. Ma, L. Cong, S. Dai and Z. Liu, *J. Organomet. Chem.*, 2018, **859**, 58–67.
39 H. Liu, W. Zhao, X. Hao, C. Redshaw, W. Huang and W.-H. Sun, *Organometallics*, 2022, **30**, 2418–2424.
40 Y. Gong, S. Li, Q. Gong, S. Zhang, B. Liu and S. Dai, *Organometallics*, 2019, **38**, 2919–2926.

 This journal is © The Royal Society of Chemistry 2023

Open Access Article. Published on 08 ubat 2023. Downloaded on 12.07.2024 02:43:51.
This article is licensed under a Creative Commons Attribution 3.0 Unported Licence.

41 R. C. Chapleski, J. L. Kern, W. C. Anderson, B. K. Long and S. Roy, *Catal. Sci. Technol.*, 2020, **10**, 2029–2039.
42 R. Tanaka, K. Sogo, K. Komaguchi, K. Ae, Y. Nakayama and T. Shiono, *Organometallics*, 2022, **41**, 3024–3031.
43 J. Xiong, W. Xie, J. Sun, J. Wang, Z. Zhu, H. Feng, D. Guo, H. Zhang and Y. Zheng, *J. Org. Chem.*, 2016, **81**, 3720–3726.
44 G. M. Sheldrick, *Acta Crystallogr., Sect. A: Found. Adv.*, 2015, **71**, 3–8.
45 G. M. Sheldrick, *Acta Crystallogr., Sect. C: Struct. Chem.*, 2015, **71**, 3–8.
46 A. L. Spek, *Acta Crystallogr., Sect. C: Struct. Chem.*, 2015, **71**, 9–18.
47 J. Tao, J. P. Perdew, V. N. Staroverov and G. E. Scuseria, *Phys. Rev. Lett.*, 2003, **91**, 146401.
48 M. J. Frisch, G. W. Trucks, H. B. Schlegel, G. E. Scuseria, M. A. Robb, J. R. Cheeseman, G. Scalmani, V. Barone, G. A. Petersson, H. Nakatsuji, X. Li, M. Caricato, A. V. Marenich, J. Bloino, B. G. Janesko, R. Gomperts, B. Mennucci, H. P. Hratchian, J. V. Ortiz, A. F. Izmaylov, J. L. Sonnenberg, D. Williams-Young, F. Ding, F. Lipparini, F. Egidi, J. Goings, B. Peng, A. Petrone, T. Henderson, D. Ranasinghe, V. G. Zakrzewski, J. Gao, N. Rega, G. Zheng, W. Liang, M. Hada, M. Ehara, K. Toyota, R. Fukuda, J. Hasegawa, M. Ishida, T. Nakajima, Y. Honda, O. Kitao, H. Nakai, T. Vreven, K. Throssell, J. A. Montgomery Jr., J. E. Peralta, F. Ogliaro, M. J. Bearpark, J. J. Heyd, E. N. Brothers, K. N. Kudin, V. N. Staroverov, T. A. Keith, R. Kobayashi, J. Normand, K. Raghavachari, A. P. Rendell, J. C. Burant, S. S. Iyengar, J. Tomasi, M. Cossi, J. M. Millam, M. Klene, C. Adamo, R. Cammi, J. W. Ochterski, R. L. Martin, K. Morokuma, O. Farkas, J. B. Foresman and D. J. Fox, *Gaussian, Inc*, Wallingford CT, 2016.
49 S. Grimme, J. Antony, S. Ehrlich and H. Krieg, *J. Chem. Phys.*, 2010, **132**, 154104.
50 S. Grimme, S. Ehrlich and L. Goerigk, *J. Comput. Chem.*, 2011, **32**, 1456–1465.